Received: 8 October 2021 | Revised: 16 December 2021 | Accepted: 6 February 2022

DOI: 10.1002/app.52370

ARTICLE

Applied Polymer Science WILEY

Preparation and characterization of innovative poly (butylene adipate terephthalate)-based biocomposites for agri-food packaging application

Corrado Sciancalepore[1,2] | Elena Togliatti[1,2] | Alberto Giubilini[2,3] | Diego Pugliese[2,3] | Fabrizio Moroni[1] | Massimo Messori[2,3] | Daniel Milanese[1,2]

[1]Dipartimento di Ingegneria e Architettura, Università di Parma, Parma

[2]INSTM, Consorzio Interuniversitario Nazionale per la Scienza e Tecnologia dei Materiali, Firenze

[3]Dipartimento di Scienza Applicata e Tecnologia, Politecnico di Torino, Torino, Italy

Correspondence
Corrado Sciancalepore, Dipartimento di Ingegneria e Architettura, Università di Parma, Parco Area delle Scienze 181/A, 43124 Parma, Italy.
Email: corrado.sciancalepore@unipr.it

Funding information
Università degli Studi di Parma

Abstract

The present work reports on the preparation and subsequent mechanical, morphological and thermal characterization of composites based on poly(butylene adipate terephthalate) (PBAT), reinforced with micro-particles of inorganic bioabsorbable calcium-phosphate glass (CPG) at different contents up to 40 wt %. The PBAT-CPG composites were prepared by solvent casting. The resulting composite pellets were used for the injection molding of model 1BA specimens, according to standard UNI EN ISO 527. PBAT-CPG composites displayed an effective increase of the Young's modulus (E) up to 82% compared to the pristine polymer, while showing a reduction of the yield stress (σ_y) up to 20%, of the stress at break (σ_B) up to 46%, of the strain at break (ε_B) up to 57% and of the toughness (T) up to 72%. The values of E, σ_y and σ_B were also compared and validated with theoretical values calculated using Kerner's and Pukanszky's models. Scanning electron microscopy (SEM) images display homogeneous dispersion and distribution of the filler particles in the polymer matrix with no aggregates or phase separation that would cause a deterioration of the material properties. Infrared (IR) spectroscopy did not show structural variations of the polymer matrix due to the CPG presence. The oxygen permeability in PBAT-based samples assumes significantly lower values when benchmarked with the permeability of low-density polyethylene (LDPE). Among the different composites, a decrease in oxygen permeability is observed as the CPG concentration increases. Regarding water vapor permeability, PBAT-based samples show a lower barrier effect than polyethylene (PE): in particular, permeability to water vapor assumes an increasing trend as the quantity of filler increases. The tuneable degradation of the final composite materials was defined by the disintegration degree (DD) determination under composting conditions in a laboratory-scale reactor. The developed materials prove to be valid biodegradable and eco-friendly alternatives to traditional

thermoplastic polymers, such as LDPE, and can be applied in many fields, especially in package and mulch film applications.

KEYWORDS

biopolymers and renewable polymers, composites, mechanical properties, microscopy, thermoplastics

1 | INTRODUCTION

Plastic materials have been used for decades in the packaging sector and beyond, thanks to their good mechanical properties, such as stiffness, lightness, barrier properties and not least their low cost. In fact, they constitute the second category of materials most used in the packaging sector, preceded by cellulosic materials.[1] Together, the plastic raw materials producers, plastics converters, plastics recyclers, and machinery manufacturers, represent a value-chain that employs over 1.5 million people in Europe, through more than 55,000 companies, most of them small medium enterprises (SMEs), operating in all European countries. In 2019, these companies created a turnover of over 350 billion euros and contributed to more than 30 billion euros to European public finances.[2] The demand and global production of plastics are constantly increasing, despite the growth curve is slightly flattening: in 2019, the world production of plastics was 368 million tons, nine more than the previous year corresponding to an increase of 2.5%.[2] Of the total production in 2019, 57.9 million tons constitute European production, corresponding to 16% of the world total. In 2019, the demand from European plastic converters was 51.2 million tons, of which about 40% went to packaging market and with higher demand for polypropylene (PP), LDPE, high-density polyethylene (HDPE) equal to 19.4, 17.4 and 12.4%, respectively.[3] The negative side of plastic commodities is represented by their fossil origin, a non-renewable source, and often also by their end-of-life, if not properly disposed and recycled. Frequently for food packaging, in order to optimize the preservation of the organoleptic food characteristics, multi-material packaging solutions are used, the recycling of which is not cost-effective and sustainable. Generally, for these kinds of plastic materials the energy valorization or the landfill disposal is adopted. Packaging, and not only food packaging, represents most of post-consumer plastic waste, approximately 63% in 2015.[4]

Furthermore, a serious problem remains the plastic waste dispersion in the environment, causing the death of fauna and the creation of large plastic islands in the sea, due to the accumulation of waste (called "plastic litter") transported by sea currents. In the European Union, up to 85% of marine litter found on beaches is made up of plastic: disposable plastic objects represent 50% of the total. The most commonly found waste included containers and lids for food and beverages and filters for tobacco products.[5] Furthermore, the fragmentation of materials causes the formation of non-biodegradable microplastics that pollute the water and the soil, with the possibility of going up the food chain starting from microorganisms. The presence of microplastics has already been reported in seafood, salt, honey, beer and even in drinking water.[5]

Although significant efforts are being made to reduce plastic components, it is currently hard to decrease the use of plastics, particularly in specific sectors, such as packaging, where no other materials are able to compete in terms of flexibility, cost and performance. Therefore, in order to find more sustainable alternatives to fossil-based plastic products, attention can be turned to the constantly expanding bioplastics sector. Bioplastics offer a series of advantages for environmental conservation and sustainability, thanks to their harmless effects on the environment and the circularity in the production system.[6] The term "bioplastics" refers to polymers which are bio-based (from renewable sources but not necessarily biodegradable), biodegradable (also with fossil origin), or have both characteristics (from renewable resources and biodegradable).[7]

PBAT belongs to the second subset of bioplastic materials. Indeed, PBAT is a synthetic polymer of the aliphatic-aromatic *co*-polyesters family, fossil-based but completely biodegradable. It is obtained through a polycondensation reaction of butanediol (BDO), adipic acid (AA) and terephthalic acid (PTA).[8]

Even if oil-based, experimental evidence shows the possibility to obtain PBAT monomers from renewable sources, making this polymer even more interesting in terms of environmental sustainability.[9–11] Thanks to its full biodegradability, PBAT is expected to undergo complete biodegradation in soil over a period of 6 weeks at 25 °C in the dark[12,13] unlike polylactic acid (PLA), where industrial fermentation conditions (60 °C) are required for its biodegration.[14]

PBAT is a flexible material with mechanical properties similar to LDPE.[15] Therefore, PBAT can be melt-

processed on standard polyolefin equipment and it can be mainly used in film applications like organic waste bags, mulch films, shopping bags, and cling films, which today are almost the exclusive prerogative of traditional non-biodegradable commodity polymers.[13]

Due to its peculiar properties and its complete biodegradability, as well as to a clear trend to renewable raw materials, PBAT can be used as an "enabler" for renewable and sustainable biopolymers and biocomposites. However, biodegradable polymers have defined property profiles, which limit their application range to some extent. If the market demands biodegradable polymer-based solutions in a circular and eco-sustainable economic approach, a composite can be developed using a combination of rigid fillers and soft biodegradable synthetic polymers, with a precise properties adjustment to the application requirements. In fact, the addition of rigid fillers is a useful way to enhance the final performance of polymers, reducing the overall material cost and ensuring the total biodegradability of the material. The reinforcement of flexible polymer matrices such as PBAT has the purpose to expand its application field especially in the food and agricultural packaging sector,[8] thanks to the similarity of PBAT properties with PE,[16] as an eco-friendly alternative to traditional oil-based polymers, very often not properly recycled or discarded.

Usually, biocomposites are fabricated by three main methods: in-situ polymerization, melt mixing and solvent casting. Materials prepared by solvent casting show optimized properties, since the liquid environment provides the two phases with the most favorable conditions to mix homogeneously and to maximize possible interactions at the interface.[17]

The preparation of PBAT-based composites has been reported by several research groups using mainly different natural fillers,[18] such as cellulose micro/nanocrystals,[19–21] montmorillonites,[22,23] natural fibers,[24–26] coffee grounds,[27] flax shive[28] and pine resin derivates.[29] The use of ceramic fillers, such as silica[30,31] or zinc[32] and magnesium oxide[33] nanoparticles, which do not guarantee the composite degradability, is less frequent. In particular, this work aims to prepare and characterize PBAT-based composites, using for the first time bioabsorbable calcium-phosphate glass (CPG) as reinforcing ceramic particles.[34,35] CPG is distinguished from traditional glass as its structure is based on phosphate (PO_4^{3-}) instead of silicate (SiO_4^{4-}) tetrahedra. CPG exhibits the important characteristic of complete biodegradability and solubility in aqueous media which can be modified by varying the glass composition,[36] thus ensuring the complete and tuneable degradability of the final composite material, while preserving a considerable mechanical reinforcement due to the high elastic modulus typical of ceramic materials.

The main techniques used to monitor the biodegradation process of bioplastic materials under aerobic and anaerobic conditions are mainly based on four methods of degradation analysis: CO_2 measurements, spectroscopy, visual analysis and mass loss methodologies.[37]

To test the biodegradation of biocomposites under aerobic composting conditions, the International Standard ISO 20200 was used, by means of the disintegration degree (DD) determination during composting in a laboratory-scale reactor. The measurement of experimental mass loss, due to the pieces extracted from samples during the testing period, is considered as an index of degradation and allows to follow the degradation process by assessing the DD, generally measured in aerobic conditions by the percentage of particles which are retained on a sieve of 2 mm. In order to compare the biocomposite behavior with the traditional plastic response to aerobic composting, a sample of LDPE was tested under the same conditions and environment.

A solvent casting manufacturing process was studied and developed, leading to the preparation of biocomposite materials, in the form of pellets, with different filler concentrations, at 0, 2, 4, 10, 20 and 40 wt%, respectively. The present work is to be considered as part of a feasibility and research step, prelude to a future phase that will involve the preparation of composite materials with more eco-friendly and industrially scalable technologies such as twin-screw extrusion, which in no way involves the use of solvents. Biocomposite pellets were further processed by injection molding to produce standard size specimens, subsequently used for mechanical, microstructural and functional characterizations. The obtained results suggest that CPG-filled PBAT-based composites represent a valid biodegradable substitute for traditional thermoplastic polymer materials with potential application especially in the agri-food packaging sector.

2 | MATERIALS AND METHODS

2.1 | Masterbatch preparation

PBAT was purchased from MAgMa Spa (Italy) as granules with a diameter of about 3 mm. The chemical–physical characteristics of the polymer are reported in Table 1.

The biodegradable CPG powder, with composition 50 P_2O_5–10 CaO–23 MgO–11.5 Na_2O–2.5 B_2O_3–3 SiO_2 (in mol%), was prepared by the traditional melt-quenching route as described in a previous work.[35] Briefly, a blend of oxides and carbonates was weighed and mixed within a dry box and the batched chemicals were melted in an alumina crucible at a temperature of 1200 °C under

TABLE 1 PBAT characteristics from the technical data sheet

Property	Unit	Value
Melt flow rate	g/10 min	≤5
Density	g/cm^3	1.26
Tensile strength	MPa	≥17
Melting temperature	°C	110–120
Elongation at break	%	≥600
Vicat softening temperature	°C	89

Abbreviation: PBAT, poly(butylene adipate terephthalate).

TABLE 2 Injection molding process settings

Temperature	
Under hopper temperature	80 °C
Plasticizing screw and barrel temperature	130 °C
Accumulation room temperature	135 °C
Nozzle temperature	130 °C
Mold temperature	15 °C
Injection	
Injection rate	55 mm/s
Injection pressure	120 bar
Shot size	27 cm^3
Plasticizing screw rotation speed	50 rpm
Maintenance after injection	
Maintenance pressure	60 bar
Maintenance time	5 s

controlled atmosphere. After 1 h, the melt was quenched onto a cold aluminium plate and the resulting glass fragments were first ground into powder by an overnight ball-milling process (Pulverisette 0, Fritsch, Idar-Oberstein, Germany) and then sifted (stainless steel sieve, Giuliani Technology Srl, Turin, Italy) in order to get a final particle size below 45 μm.

The preparation of the PBAT-CPG composites was carried out by a solvent casting approach, using chloroform ($CHCl_3$—Sigma-Aldrich) as suitable solvent. To obtain the composite materials, the main steps were the dissolution of the polymer in the solvent and the dispersion of the filler particles in the polymer solution, followed by $CHCl_3$ evaporation with the formation of solid films, and pellets production. The polymer solution with the dispersed CPG particles in $CHCl_3$ was casted onto a non-stick surface and spread with a spatula to reduce the thickness and facilitate the evaporation of the solvent. After 12 h under an extractor hood, the films were manually reduced to pellets. Finally, the pellets were heat-treated at 80 °C up to a constant weight. The weight fraction of the CPG fillers varied from 0 to 40 wt%, thus obtaining composites at different filler concentrations, in order to evaluate the variation in the material properties as a function of the CPG content.

The resulting pellets were used for the injection molding of dumbbell specimens, model 1BA, according to UNI EN ISO 527 standard for tensile characterization. A MegaTech H7/18-1 machine (Tecnica Duebi, Italy) was employed for the injection molding process.

The process parameters, set for the specimen molding, are summarized in Table 2.

The obtained samples, containing respectively 0 (pure PBAT), 2, 4, 10, 20, 40 wt% of CPG, are named as PBAT, PBAT+2% CPG, PBAT+4% CPG, PBAT+10% CPG, PBAT+20% CPG, PBAT+40% CPG.

2.2 | Tensile test

The uniaxial tensile tests were performed with a TesT dynamometer (Model 112, TesT GMBH Universal Testing Machine, Germany). Measurements were carried out at a constant tensile speed of 100 mm/min until the sample broke. E, σ_y, σ_B, ε_B and T were expressed as average values on at least seven different acquisitions for each composite material.

Further tensile tests were also conducted for the determination of PBAT Poisson's ratio, obtained by means of a digital image correlation (DIC) technique. Tests were carried out at a constant tensile speed of 5 mm/min and pictures of the specimen portion were taken using a 5 MPx Dinolite digital camera (Almere, The Netherlands), approximately every 0.01 mm/mm of elongation (Figure 1).

The images were then processed using the DICe open-source software [Turner, D.Z. Digital Image Correlation Engine (DICe) Reference Manual, Sandia Report, SAND2015-10606 O, 2015] and correlation results were examined with ParaView visualization software.[38]

The distance between two points aligned to the loading direction (L_X) and the distance between two points orthogonally aligned to the load direction (L_Y) were monitored, and the value of longitudinal (ε_X) and transversal (ε_Y) strains were computed as follows: $\varepsilon_X = \frac{L_{Xi}}{L_{Xi}-L_{X0}}$ and $\varepsilon_Y = \frac{L_{Yi}}{L_{Yi}-L_{Y0}}$, where the subscript "0" refers to the initial distance and the subscript "i" refers to the actual distance during the test.

Finally, the Poisson's ratio was computed as the slope of the best fit linear regression of the plot $-\varepsilon_Y$ versus ε_X, considering data until a longitudinal strain approximately equal to 0.08 mm/mm was reached (Figure 2). This procedure was repeated for three specimens and the

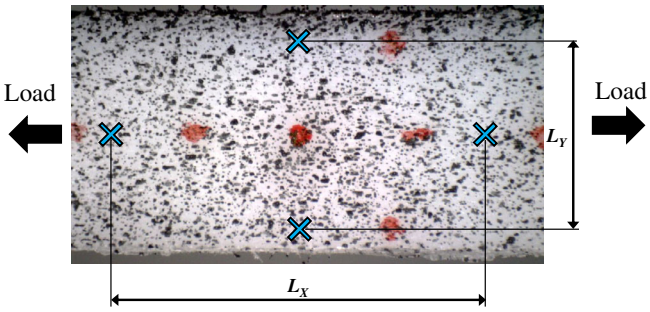

FIGURE 1 Example of the picture and of the procedure used for the PBAT Poisson's ratio estimation [Color figure can be viewed at wileyonlinelibrary.com]

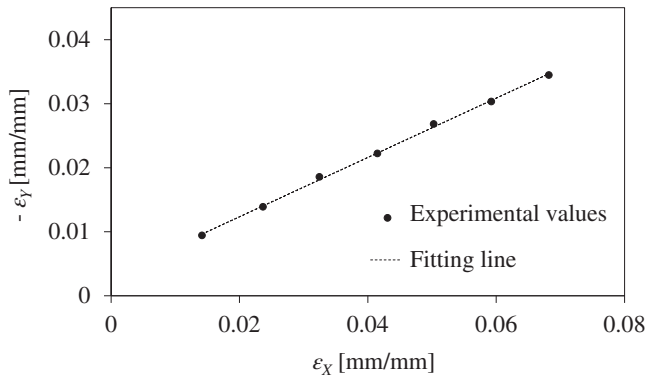

FIGURE 2 Example of the Poisson's ratio estimation from the longitudinal (ε_X) and transversal (ε_Y) strains

resulting average value of the Poisson's ratio was 0.46 ± 0.01.

2.3 | Composite modeling

In order to compare the experimental mechanical behavior of composites with theoretical models, the Kerner's equation, as proposed by Lewis and Nielsen,[39] was used to predict E values, while Pukanszky's equations were applied to obtain information about filler-matrix interaction starting from σ_y and σ_B experimental quantities.[40,41] Both models consider the properties of a composite material as a function of the filler volumetric fraction.

The generalized Kerner's equation (Equation 1) was used in the form:

$$E' = E'_1 \frac{1 + AC}{1 - C\psi\phi_2}, \tag{1}$$

where E', E'_1 are respectively the Young's moduli of composite and unfilled polymer, $\phi_2 = \frac{\frac{g_p}{\rho_p}}{\frac{g_p}{\rho_p} + \frac{g_m}{\rho_m}}$ is the filler volume fraction (ρ_p and ρ_m are respectively the filler and matrix densities, experimentally determined), and A, C and ψ are parameters defined as follows:

$$A = \frac{7 - 5\upsilon}{8 - 10\upsilon}, \tag{2}$$

where ν is the Poisson's ratio of the polymer matrix,

$$C = \frac{\frac{E_p}{E_m} - 1}{\frac{E_p}{E_m} + A}, \tag{3}$$

where E_p and E_m represent experimental values of E for CPG and PBAT, respectively,

$$\psi = 1 + \frac{1 - \phi_m}{\phi_m^2} \times \phi_2, \tag{4}$$

where ϕ_m is the maximum packing fraction of the filler (0.632 for randomly close packed non-agglomerated spherical particles[42]).

Values of material parameters, used in Kerner's equation, are summarized in Table 3.

The experimental values of E were reported on a plot as a function of the volumetric fraction of filler and compared with the theoretical values E' deriving from Equation (1).

Composite σ_y was modeled by Pukanszky's equation:[41]

$$\sigma_y = \sigma_{y0} \frac{1 - \phi_f}{1 + 2.5\phi_f} \exp(B \times \phi_f), \tag{5}$$

where ϕ_f is the CPG volumetric fraction, σ_y and σ_{y0} are the experimental yield stresses of the composite and of the matrix, respectively, and B is an empirical parameter characterizing the degree of filler-matrix interaction. The value of the parameter B depends on all the factors influencing the load-bearing capacity, i.e., strength and

TABLE 3 Values of material parameters, used in Kerner's equation

Parameter	Value	Determination method
E_m	101.87 MPa	Experimental by tensile test
E_p	53.1 GPa	Experimental in[34]
ρ_m	1.26 g/cm^3	Tabulated in PBAT data sheet
ρ_p	2.59 g/cm^3	Experimental in[34]
ν	0.46	Experimental by DIC technique
ϕ_m	0.632	Tabulated in[42]

Abbreviations: DIC, digital image correlation; PBAT, poly(butylene adipate terephthalate).

size of the interface. B generally assumes values between 2 and 15 for polymer-based micro- and nanocomposites.[41,43,44]

Equation (5) was linearized in semi-logarithmic form as follows:

$$\log\sigma_{y,rel} = \log\left(\frac{\sigma_y(1+2.5\phi_f)}{\sigma_{y0}(1-\phi_f)}\right) = B\times\phi_f. \quad (6)$$

The obtained values of relative yield stress, $\sigma_{y,rel}$, were reported as a function of the CPG volume fraction and B value was acquired as the slope of the fitting line.

Using the B value calculated for the yield stress, the modified Pukanszky's model was used for modeling the stress at break:

$$\sigma_{B,T} = \sigma_{B,T_0 rel}\lambda^n \frac{1-\phi_f}{1+2.5\phi_f}\exp(B\phi_f), \quad (7)$$

where $\sigma_{B,T}$ is the true tensile strength at break of the composite ($\sigma_{B,T} = \sigma \times \lambda$, with $\lambda = L/L_0$ the relative elongation, L the elongation measured during the tensile test and L_0 the initial length of the specimen) and accounts for the change in specimen cross-section, $\sigma_{B,T_0 rel} = \frac{\sigma_{B,T_0}}{\lambda^n}$ is the relative true value of the PBAT stress at break ($\sigma_{B,T_0} = \sigma_0 \times \lambda$), λ^n is the correction factor for strain hardening and n is a constant which characterizes the strain hardening tendency of the polymer and was experimentally determined from matrix properties.[45]

Rearranging and linearizing Equation (7), the reduced stress at break, $\sigma_{B,T\,red}$, can be represented as a function of CPG ϕ_f:

$$\log(\sigma_{B,T\,red}) = B\phi_f, \quad (8)$$

where $\sigma_{B,T\,red} = \frac{\sigma_{B,T}\,(1+2.5\phi_f)}{\lambda^n\sigma_{B,T_0 rel}(1-\phi_f)} = \exp(B\phi_f)$.

2.4 | Particle size analysis

The particle size analysis of the CPG particles was carried out using a Mastersizer 3000 laser granulometer (Malvern Instruments Ltd., Malvern, UK), in wet mode with water as dispersing medium, using Mie's theory as scattering model. The CPG particles were dispersed in water by means of the stirring system of the wet dispersion unit (Hydro EV) at a speed of 2700 rpm. The dispersion was stable throughout the measurement period required to acquire approximately 30 replicates. The dimensional distribution of the filler particles was expressed by the values of D10, D50, D90 standard percentiles, which represent respectively the size of particle below which 10, 50 and 90% of the sample lies. Standard percentiles are referred to the number distribution. The particle average size was expressed by the equivalent number mean diameter, D_{mean}.

2.5 | Infrared spectroscopy

The infrared (IR) spectra were acquired using the Perkin-Elmer Spectrum Two FT-IR spectrophotometer, in attenuated total reflectance (ATR) mode with a diamond crystal plate. Each spectrum was the average of 16 scans, acquired in the range 4000–400 cm^{-1} and with a resolution of 4 cm^{-1}.

2.6 | Scanning electron microscopy and electron dispersion spectroscopy

The microstructure of the composites at different filler concentrations and the morphology of CPG powder were analyzed by scanning electron microscopy (SEM). For SEM analysis, the investigated cross-section was achieved by sectioning the central portion of the injected samples with a sharp blade. To make the sample surface conductive, an approximately 10 nm layer of gold was applied by sputtering.

SEM characterizations were performed by means of a field emission gun SEM (FESEM, Nova NanoSEM 450, FEI company, USA). Images were acquired in field-free lens mode making use of the circular backscatter detector (CBS), to highlight the image contrast due to the sample compositional variations. The accelerating voltage (HV) of 15 kV, the spot size of 4 (a. u.) and the working distance (WD) of about 6 mm were utilized in the acquisition of all images.

Chemical elemental analysis was performed by means of the energy-dispersive X-ray spectroscopy system (EDS) QUANTAX-200 (Bruker, Germany), equipped with the silicon drift detector (SDD) XFlash 6/10.

2.7 | Differential scanning calorimetry

The thermal parameters of composites, such as glass transition (T_g), melting (T_m) and crystallization (T_c) temperatures, were obtained by differential scanning calorimetric (DSC) analysis.

A small portion (10–20 mg) of the composite samples, obtained by injection molding, was subjected to DSC analysis using a Perkin Helmer DSC6000 (PerkinElmer, USA). The heating scan was carried out in the thermal range −60/200 °C with a rate of 10 °C/min, while the cooling scan set at a rate of 10 °C/min from 200 to 0 °C.

2.8 | Permeability test

Films with dimensions of 10 × 10 cm^2 and thickness of about 0.35 mm were obtained from composite batches and compared with a LDPE film in oxygen and water vapor permeability tests. Riblene FC 39 D (supplied by Versalis S.p.A., Italy) is the commercial LDPE used for comparison.

The films were prepared by drying the pellets in a vacuum oven at a temperature of 80 °C for 4 h and subsequently processing them with a Collin P 200 T press (Collin Lab & Pilot Solutions GmbH, Germany).

The parameters used for making the films are summarized in Table 4. For LDPE, the only difference was the use of 190 °C as molding temperature.

In order to carry out the analysis of permeability to oxygen and water vapor, the permeability tester for thin film MultiPerm (Extrasolution Srl, Italy) with embedded controls of temperature and relative humidity was used. Performed tests comply with the standards ASTM D3985 and ASTM F1249 for oxygen transmission rate (OTR) and water vapor transmission rate (WVTR) measurements, respectively.

The operating conditions used for all the analyzed samples are shown in Table 5.

2.9 | Disintegration test

The disintegration of pristine PBAT, PBAT-based composites and LDPE was investigated under simulated composting conditions in a laboratory scale test as described in the EN ISO 20200 technical standard. Dry synthetic solid waste was manually prepared with the following composition: 40 wt% of sawdust (OBI Italy), 30 wt% of rabbit-feed (Vitakraft, Germany), 10 wt% of ripe compost (Vivi Verde Coop), acting as inoculum, 10 wt% of corn starch, 5 wt% of sugar, 4 wt% of cornseed oil and 1 wt% of urea (Sigma-Aldrich). After mixing, distilled water was added to the obtained synthetic solid waste to adjust its final water content to 55 wt%. The prepared compost, together with the film specimens of composite materials, were placed in PP reactors. The amount of wet synthetic solid waste used in each reactor was such as to have a ratio between the test material and the wet synthetic waste equal to 0.5 wt%.

Reactors were weighed and the total masses recorded previously to put them into an ISCO NSV 9090 oven at 58 ± 2 °C for the thermophilic incubation period. During this period the reactors were periodically weighed, the water content restored, to maintain a sufficient and constant relative humidity in the compost medium, and the compost mixed. The overall test duration was 88 days.

Three film specimens of 2.5 × 2.5 cm^2 were tested for each PBAT-based material and for LDPE as traditional plastic reference. Every week the film samples were recovered, rinsed with deionized water, dried overnight at 40 °C and weighed to monitor the fragmentation process and to calculate the corresponding disintegration degree (DD):

$$\mathrm{DD} = \left(\frac{M_0 - M_\mathrm{i}}{M_0}\right) \times 100, \tag{9}$$

where M_0 corresponds to the initial dry mass of the specimen and M_i represents the dry mass of the recovered pieces during the monitoring period.

To validate the DD, the decrease in volatile-solids content degree (R) was also calculated according to:

$$R = \frac{[m_0(\mathrm{DM}_0)(\mathrm{VS}_0)] - [m_\mathrm{f}(\mathrm{DM}_\mathrm{f})(\mathrm{VS}_\mathrm{f})]}{[m_0(\mathrm{DM}_0)(\mathrm{VS}_0)]}, \tag{10}$$

where m_0 is the initial mass of wet waste matrix, DM_0 is the dry mass of waste matrix and VS_0 the initial volatile-solids of wet waste matrix. m_f, DM_f and VS_f represent the final mass, the final dry mass and the final volatile-solids of compost at the end of test period, respectively.

TABLE 4 Film molding parameters

Molding temperature	130 °C (190 °C for LDPE)
Lamination time	3 min
Degassing cycles	10
Maintaining	100 bar for 3 min
Water cooling	100 bar until 50 °C
Air cooling	10 s

Abbreviation: LDPE, low-density polyethylene.

TABLE 5 Settings used for permeability tests

Set point temperature [°C]	23
Relative moisture [%]	1.0 ± 0.1
Carrier flow [ml/min]	12.3

3 | RESULTS AND DISCUSSION

3.1 | Tensile characterization

Figure 3 shows the specimens of the various composites obtained by injection molding, before (a) and after (b) the tensile tests. As evident from Figure 3a, the appearance

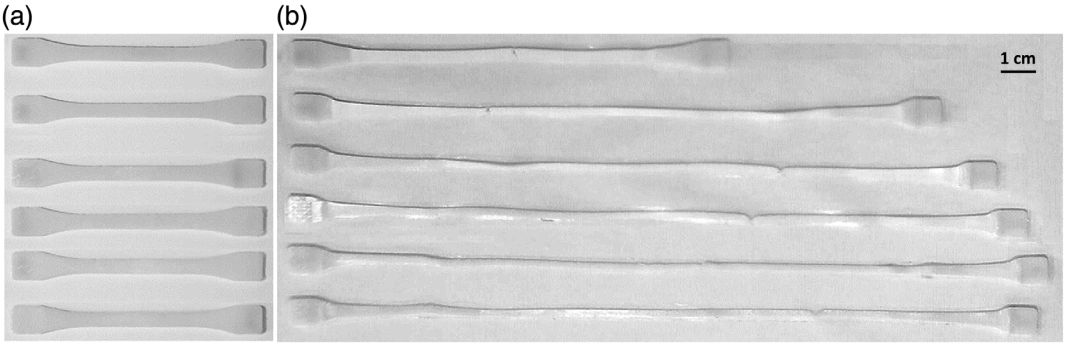

FIGURE 3 Specimens obtained by injection molding without sprue, before (a) and after (b) tensile test; from bottom to top: PBAT, PBAT+2% calcium-phosphate glass (CPG), PBAT+4% CPG, PBAT+10% CPG, PBAT+20% CPG, PBAT+40% CPG

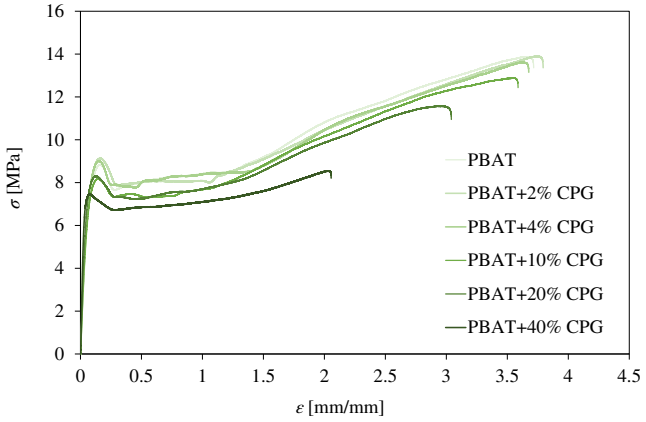

FIGURE 4 Stress–strain curves of poly(butylene adipate terephthalate) (PBAT)-based composite materials [Color figure can be viewed at wileyonlinelibrary.com]

of the specimen did not significantly change with increasing the percentage of filler.

The stress–strain curves are typical of a tough polymer material with a yield point and are shown in Figure 4.

All tensile curves are characterized by an initial linear part due to elastic deformation, followed by a second plastic deformation zone with the formation of a central neck, which spreads along the entire central section of the specimen, up to the gripping areas. In this last section, the polymer chains are aligned along the stress direction, determining a tough behavior of the material, up to failure. The presence of CPG micro-particles determines an increase in E and at the same time a reduction in σ_y, σ_B, ε_B and T. In particular, as the concentration of CPG increases, E can be observed to increase up to 82%, with a reduction of 20, 46, 54 and 72% in σ_y, σ_B, ε_B and T, respectively (Figure 5, from (a) to (e)).

As it commonly happens in polymer-based micro-composites, the introduction of micro fillers in these systems leads to an enhancement of the elastic modulus, in comparison to the neat polymer. In order to explain the elastic modulus improvement observed in bio-composite samples,[46,47] the presence of an interphase layer around the nanoparticles, promoting the stress transfer at the interface, can be hypothesized. It is also reported that the particles can restrict the mobility and deformation of the matrix by introducing a mechanical restraint.[48]

The stiffening effect provided by CPG particles can be modeled by considering the theoretical approaches developed by the generalized Kerner's model for traditional micro-composites.

According to this model, composite modulus does not explicitly depend on the particle size and particle size distribution. Both these parameters and the effect of surface treatment affect the model previsions only indirectly through the maximum packing fraction (ϕ_m).

In Figure 6 the experimental data are compared with the theoretical previsions according to Lewis-Nielsen's model. The stiffening effect of CPG particles is in good agreement with the theoretical prediction based on the modified Kerner's equation, also at high CPG amounts.

Usually, in composites filled with traditional micro fillers (chalk, calcium carbonate), the increase of the composite elastic modulus is generally associated with the decrease of the yield stress, because fillers decrease the effective cross-section of the matrix that carries the load during the deformation.[49]

More attempts are made to predict and analyze the yield stress. Pukanszky's model applies the Equation (5) for the effective load-bearing cross-section and considers the influence of interfacial interaction and interphase formation by means of B parameter, associated with the relative load-bearing capacity of the components, i.e., to interaction between filler and polymer matrix.[41]

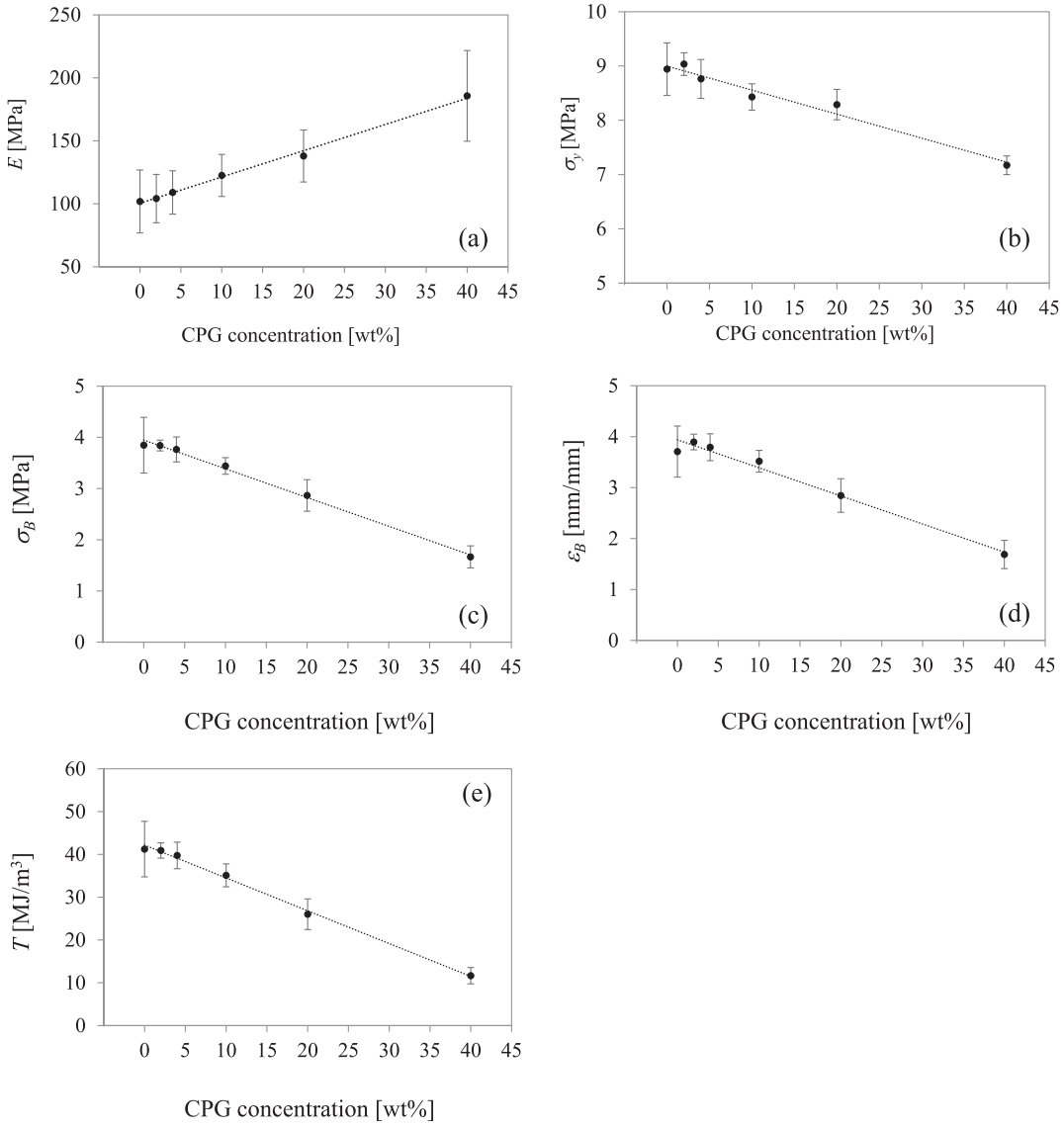

FIGURE 5 E, σ_y, σ_B, ε_B and T as a function of the calcium-phosphate glass (CPG) concentration, from (a) to (e), respectively

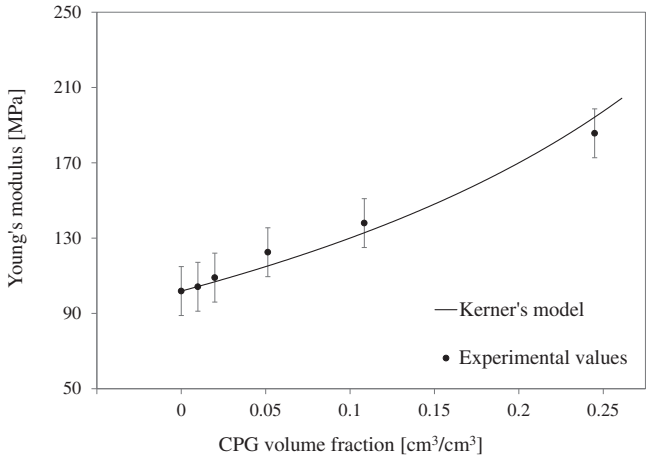

FIGURE 6 Comparison between experimental Young's moduli and the corresponding theoretical values, calculated with the Kerner's model

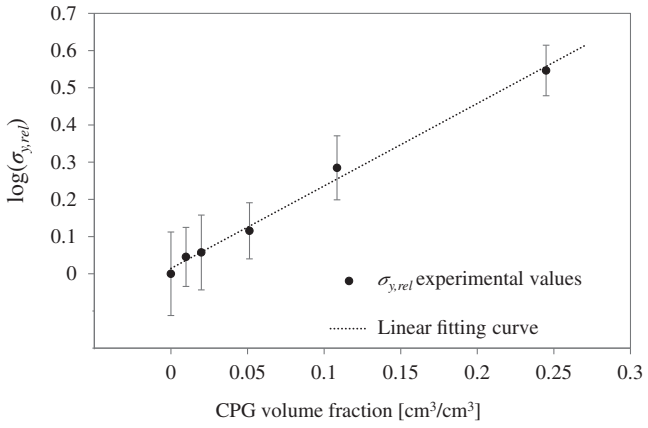

FIGURE 7 Relative tensile stress at yield, $\sigma_{y,rel}$, calculated according to the Pukanszky's model, as a function of the CPG volumetric fraction

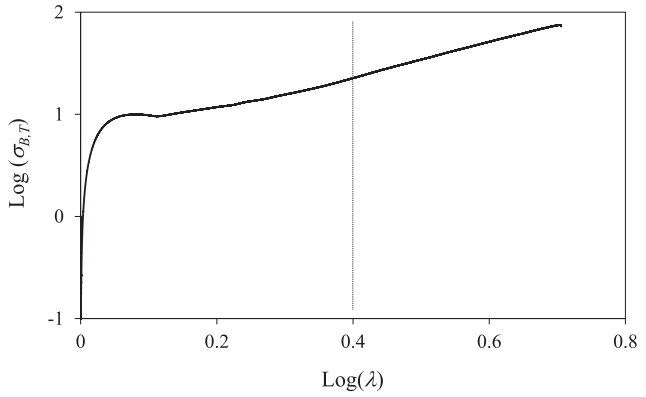

FIGURE 8 True PBAT stress–strain curve

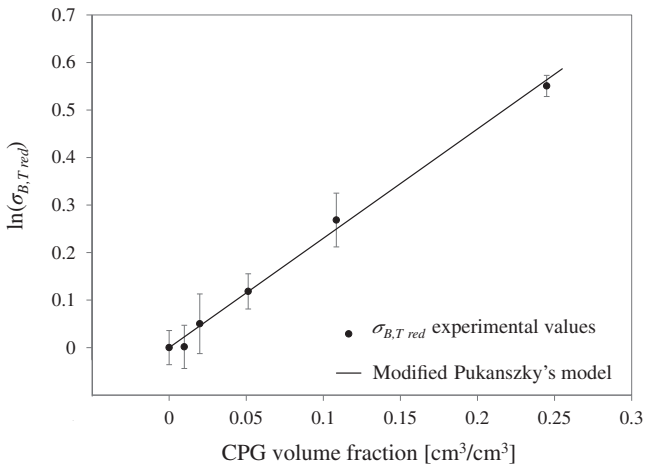

FIGURE 9 Comparison between experimental reduced stress at break, $\sigma_{B,Tred}$, and the corresponding theoretical values, calculated with the modified Pukanszky's model

In Figure 7 the relative tensile stress at yield, $\sigma_{y,rel}$, values of PBAT and relative composites according to Pukanszky's equation (Equation 6) are reported with the linear fitting line.

The slope of the fitting line represents the value of $B = 2.30 \pm 0.08$, confirming a positive relationship between PBAT and CPG. In fact this value indicates the formation of an interactive interphase between filler and matrix, in line with the values found in the literature for traditional rigid fillers.[40] If B assumes low values, it indicates a poor interaction between the matrix and the filler particles, resulting in a reduction of the mechanical properties of the composite as the percentage of filler increases. Indeed, the stress would result mainly on the matrix, which takes on a gradually lower percentage in the composite. Conversely, if the values assumed by B are high, the matrix and filler will exhibit a high degree of interaction and consequently the composite will have an improved mechanical behavior.

Numerous authors have previously investigated the behavior of different polymer-based composites reinforced with micro- and nano-metric particles. Generally, the value of B for polymer-based micro- and nano-composites assumes values between 2 and 15.[30,44,50]

The dependence of the tensile strength at break is very similar to that of the yield characteristics. Usually, strength at break decreases with increasing filler content.[51] The number of models predicting ultimate properties is even smaller than for yield stress or yield strain. The models developed by Pukanszky for yield properties can be applied also for strength at break, accounting the true tensile strength ($\sigma_{B,T} = \sigma \times \lambda$, with $\lambda = L/L_0$ the relative elongation) for the change in specimen cross-section and λ^n for strain hardening (Equation 7).[45] n characterizes the strain hardening tendency of the polymer and is experimentally obtained from the true PBAT stress–strain curve, reported in Figure 8.

The curve section with $\log(\lambda) > 0.4$ has a constant slope. This slope represents the value of $n = 1.703$, used to obtain the reduced stress at break, $\sigma_{B,Tred}$, as expressed in Equation (8).

Factor B for stress at break is defined by a correlation like the one used for yield stress[41] and its value, used in the modified Pukanszky's model (defined by Equation 7), is the same as calculated for the yield stress.

In Figure 9 the experimental values $\sigma_{B,Tred}$ are reported in a semilogarithmic plot and compared with the theoretical function of Pukanszky. A remarkable correspondence is found between the experimentally obtained values and the theoretical model, whose values do not differ significantly and fall within the experimental standard deviation.

3.2 | FESEM and EDS characterization

Microstructural composite morphology is a key parameter to support the observed mechanical properties of polymer composites. Backscattered FESEM micrographs of composites at different filler content are reported in Figure 10 and reveal the presence of CPG particles with a higher image contrast and therefore with a different composition compared to the polymer carbon-based matrix.

FESEM images highlight homogeneous dispersion and distribution of the filler particles in the polymer matrix with no aggregates or phase separation that would cause the unraveling of the material properties.

Even at high filler concentrations, no voids at the interface can be noted, indicating a good surface wettability and compatibility of CPG particles with the polymer matrix.

CPG particles show an irregular geometry and are generally smaller than 10 μm in size, as shown by

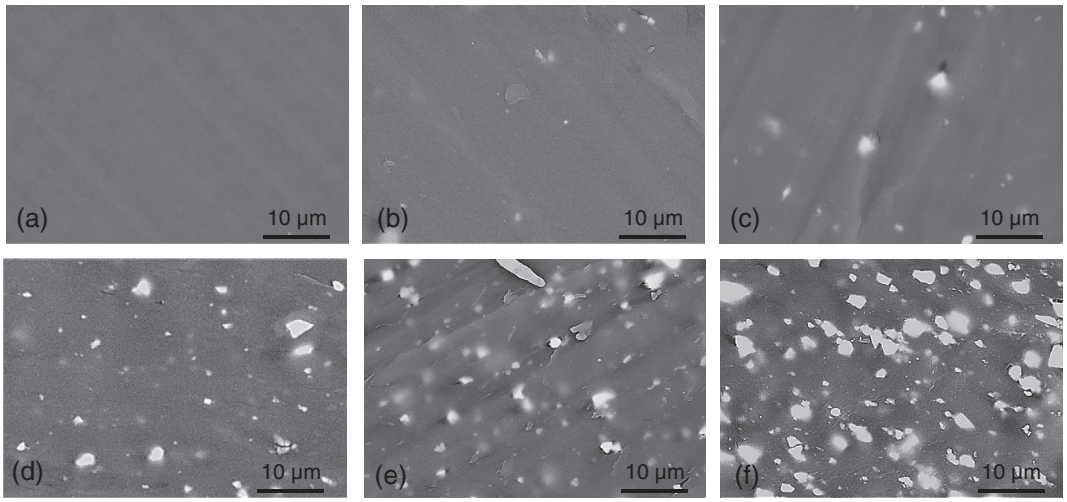

FIGURE 10 FESEM images of PBAT (a), PBAT+2% calcium-phosphate glass (CPG) (b), PBAT+4% CPG (c), PBAT+10% CPG (d), PBAT+20% CPG (e), PBAT+40% CPG (f)

FIGURE 11 FESEM image of CPG grains (a) and their size distribution (b)

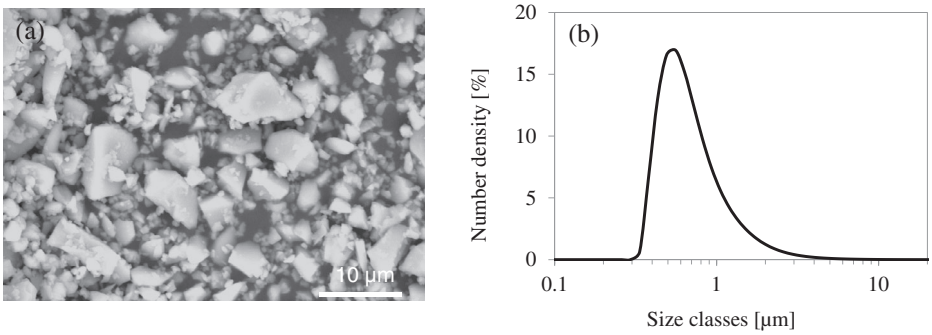

FESEM image in Figure 11a. This observation is confirmed by the particle size measurements (Figure 11b), indicating a particle average value of 0.781 ± 0.001 μm and D10, D50 and D90 values equal to 0.426, 0.625 and 1.250 μm, respectively.

In Figure 12 EDS spectra of all composites and CPG are reported. As CPG concentration increases, the intensity of the polymer characteristic peaks (in particular C peak) decreases and at the same time the CPG characteristic peaks (P, Ca, Na, K, Al and Si) increase. The intensity of the O peak does not undergo significant variations as the decrease in intensity regarding the polymer matrix is compensated by an increase in intensity referring to the glass content.

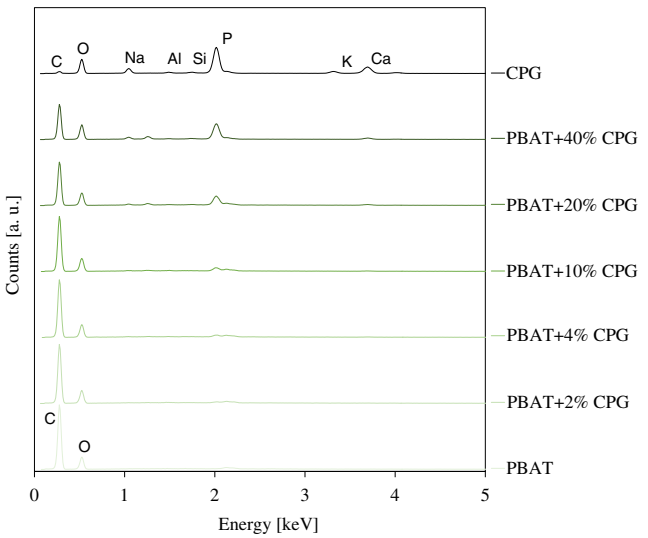

FIGURE 12 EDS spectra of PBAT-based composites and CPG particles [Color figure can be viewed at wileyonlinelibrary.com]

3.3 | IR spectroscopy characterization

Figure 13 shows IR spectra of composite samples with increasing CPG concentration and pure CPG powder, in order to obtain structural information on the polymer matrix and possible variations due to the interactions between polymer chains and CPG particles.

PBAT and CPG characteristic peaks are summarized in Table 6.[52–54] In particular, the characteristic band of the carbonyl functional groups shows a shoulder at

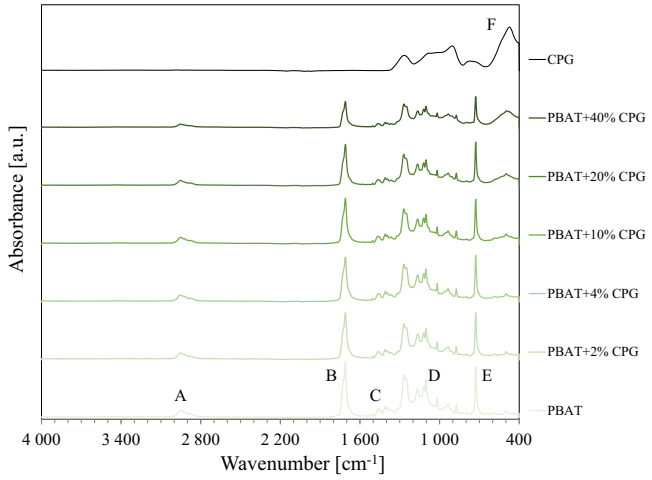

FIGURE 13 Infrared (IR) spectra of PBAT-based composites and CPG grains [Color figure can be viewed at wileyonlinelibrary.com]

higher wavenumbers than the main peak. The blue shift is due to the carbonyl moiety in the adipate ester group, which does not present conjugative effect, such as in the terephthalate unit between phenylene and carbonyl groups.[55,56] Moreover, always in the terephthalate unit, the strong band due to the aromatic ring out-of-plane deformation is not in its normal position for para-substituted aromatics, instead it is found at slightly lower wavenumbers, 725 cm^{-1}. This shift is attributed to an interaction of the ester group with the aromatic ring.[57]

Based on the spectroscopic evidence, as the concentration of glass increases, a general decrease in the intensity of the PBAT absorption peaks and an increase in the CPG band at 520 cm^{-1} can be observed. No particular structural variations are detected due to possible interactions of the CPG with the polymer matrix.

TABLE 6 Characteristic wavenumbers of IR peaks for PBAT-based composites and CPG

A	2800–2900 cm^{-1}	Symmetric and asymmetric stretching of methylene (—CH_2—) group in adipate and 1,4-butanedienol units
B	1700 cm^{-1}	Stretching of the carbonyl (C═O) group in the adipate and terephthalate units
C	1600–1450 cm^{-1}	Stretching of the double bonds (C═C) in the aromatic ring of terephthalate unit
D	1300–1000 cm^{-1}	Asymmetric stretching of (C—O) bond in ester group
E	725 cm^{-1}	Out-of-plane C—H bending in the aromatic ring of terephthalate unit
F	520 cm^{-1}	Bending vibration of P—O bond

Abbreviations: CPG, calcium-phosphate glass; IR, infrared; PBAT, poly(butylene adipate terephthalate).

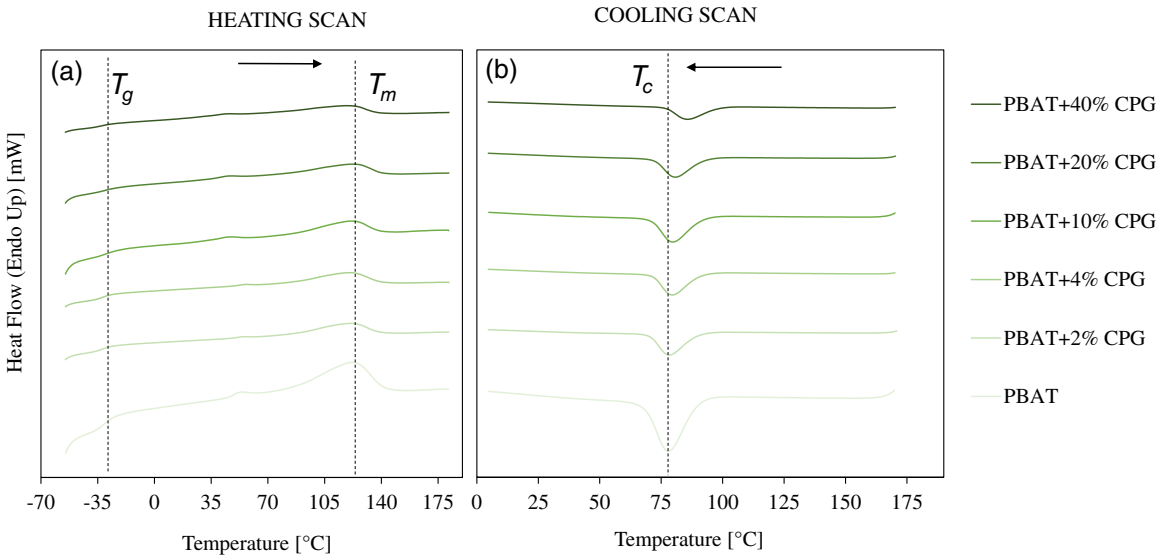

FIGURE 14 DSC thermograms of PBAT-based composites: heating (a) and cooling (b) scans, respectively [Color figure can be viewed at wileyonlinelibrary.com]

3.4 | DSC characterization

Figure 14 represents the two phases of the DSC analysis carried out on the composite material samples: the heating (Figure 14a) and cooling (Figure 14b) scans, respectively.

Observing the trend of the characteristic temperatures as a function of the CPG content, during the heating scan, the glass transition temperature, T_g, and the melting temperature, T_m, maintain approximately constant values, at about −30 and 120 °C, respectively. A slightly more marked trend is reported by the crystallization temperature, T_c, during the cooling scan, showing increasing values with the CPG percentage in the range of 78–85 °C.

In the case of the T_c, it can be assumed that the CPG particles hinder the movement of the polymer chains and at the same time act as nucleating agent for PBAT macromolecules.[58,59] Consequently, the attractive intermolecular forces become more and more relevant at higher temperatures. The result is an increase in the T_c value, as the percentage of added CPG increases.

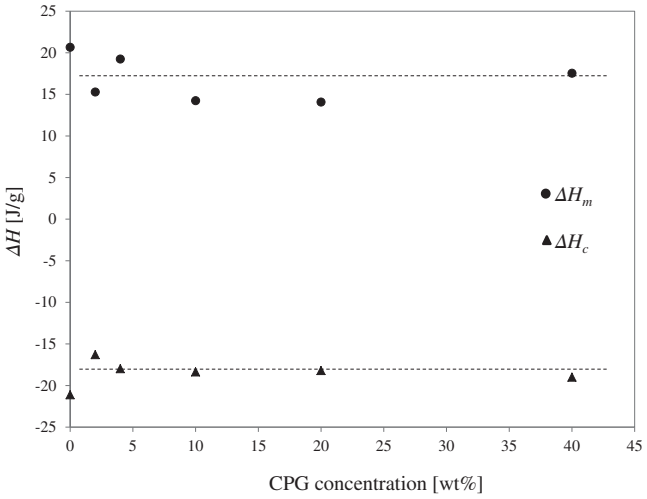

FIGURE 15 Melting and crystallization enthalpies as a function of the CPG concentration

The normalized values of melting, ΔH_m, and crystallization, ΔH_c, enthalpies are reported in Figure 15 and show that the enthalpy variation can be considered negligible, independently from CPG concentration. Consequently, it is possible to state that the addition of CPG particles does not change PBAT thermal properties.

3.5 | Permeability characterization

The results of the permeability tests are presented in Table 7 and in Figure 16, showing the oxygen (Figure 16a) and water vapor (Figure 16b) permeabilities, respectively.

Although the trend is only indicative as the values are within the standard deviations, the oxygen and water vapor permeabilities appear to depend proportionally on the CPG content.

Regarding oxygen permeability, considerably lower values are observed in the pure PBAT and in the composites when compared to permeability values of PE.[60] In addition, the CPG fillers increase the barrier properties of the composite materials, showing a decreasing trend in oxygen permeability as the CPG content increases.

Considering the water vapor permeability, PBAT-based materials display higher permeability values by over an order of magnitude compared to PE and with an increasing trend as the quantity of filler increases: PBAT and the related composites exhibit therefore a lower barrier effect to humidity compared to PE.

The gas and vapor permeability of PBAT is substantially linked to the polar nature of the bonds present in the polymer chain, unlike PE in which the macromolecular chain is substantially apolar. Hence, strongly polar molecules such as water, characterized by the O—H bond, are more compatible with ester group in PBAT and therefore permeate and diffuse in the polymer more easily, while structurally symmetrical molecules, lacking a strong electric dipole, such as the molecule of oxygen

TABLE 7 Oxygen and water vapor permeability values for PE and PBAT-based composite films

Sample	Film thickness [mm]	Oxygen permeability [cc mm/(m² 24 h atm)]	Water vapor permeability [g mm/(m² 24 h atm)]
PE	0.57	153 ± 5	0.10 ± 0.05
PBAT	0.34	68 ± 5	3.3 ± 0.2
PBAT + 2% CPG	0.35	66 ± 5	3.3 ± 0.2
PBAT + 4% CPG	0.41	67 ± 5	3.6 ± 0.2
PBAT + 10% CPG	0.37	60 ± 4	3.3 ± 0.2
PBAT + 20% CPG	0.36	53 ± 4	3.7 ± 0.3
PBAT + 40% CPG	0.40	60 ± 4	4.5 ± 0.3

Abbreviations: CPG, calcium-phosphate glass; PBAT, poly(butylene adipate terephthalate); PE, polyethylene.

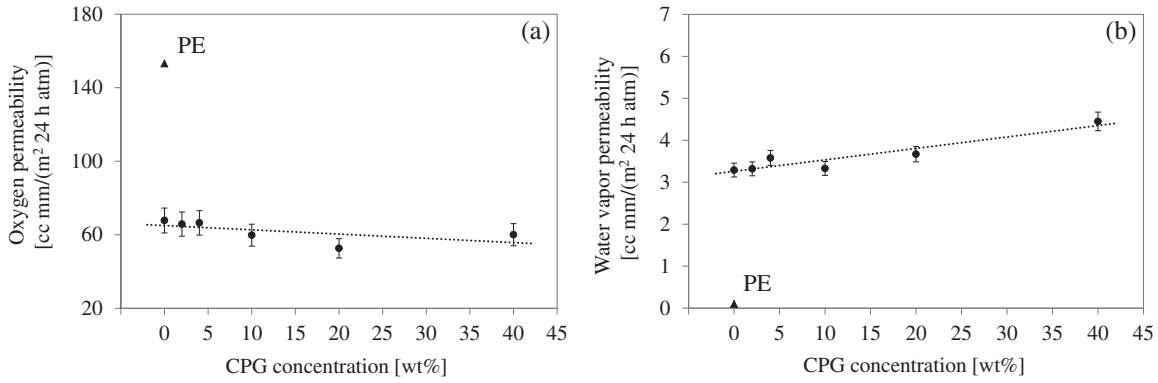

FIGURE 16 Oxygen (a) and water vapor (b) permeability as a function of the CPG concentration. The PE permeability values have been added for the sake of comparison

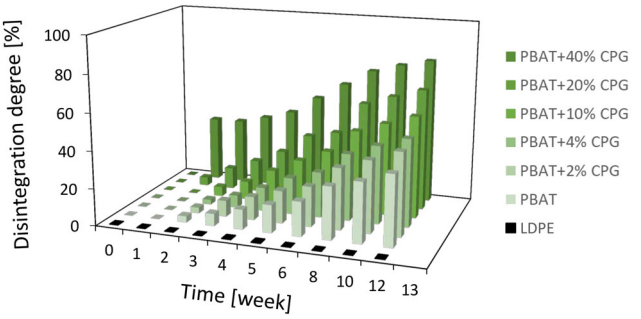

FIGURE 17 Disintegration degree of the poly(butylene adipate terephthalate) (PBAT)-based composites and low-density polyethylene (LDPE) as a function of time and material composition [Color figure can be viewed at wileyonlinelibrary.com]

(O═O) or carbon dioxide (O═C═O), permeate the polymer with more difficulties. It follows that the polymers with polar functionality, like PBAT, allow water vapor to pass through much more, while they show a lower oxygen permeability. In the presence of polar inorganic structures such as CPG, this behavior is even more evident. In fact, CPG is soluble in aqueous environments, so it makes sense to expect water vapor permeability to increase in composites with a higher filler content.

The main purpose for which the CPG addition to PBAT matrix was carried out is to increase and tune the rigidity of the material, rather than improving the barrier effect. The results obtained from the permeability tests, especially regarding oxygen permeability, constitute a further advantage in the use of PBAT-based biodegradable composites, designed to replace PE in packaging applications. Furthermore, the high water vapor permeability does not necessarily represent a disadvantage: previous studies have found that, compared to an LDPE film, the humidity produced by the vegetable metabolic activity has the possibility to better spread through the packaging film, resulting in the absence of condensation inside the package and thus reducing the risk of mold development.[61]

3.6 | Disintegration characterization

The measurement of experimental mass loss from film specimens subjected to aerobic conditions degradation during the testing period can be considered as an index of the material degradation capacity by assessing the DD. According to ISO 20200, DD is measured experimentally by the percentage of particles that are retained by a 2 mm metal mesh, washed with distilled water, dried at 40 °C and weighed.

Figure 17 displays the DD of the PBAT-based composites and LDPE as a function of time and material composition. The DD of pristine PBAT and related composites indicates an evident growing trend over the composting time. In particular, the DD increases as the filler content in the polymeric matrix increases. CPG particles seem to affect the disintegration process of the biopolymer, thereby increasing the degradability of the composites, depending on their content. The same behavior has already been observed for bio-based composite materials loaded with cellulose nanocrystals, where the nanofillers would promote the diffusion and contact of the water molecules with the polymeric matrix promoting the hydrolysis of the polymer chains into smaller molecules more easily metabolized by microorganisms.[62]

The PBAT degradation process occurs mainly by hydrolytic dissociation of the ester bond present in the polymer chain.[63] The hydrophilic character of the CPG particles, uniformly distributed in the polymeric matrix, could favor this reaction following a greater and faster absorption of water molecules by the composite material. Furthermore, the solubilization of the CPG particles in the composting environment would determine the

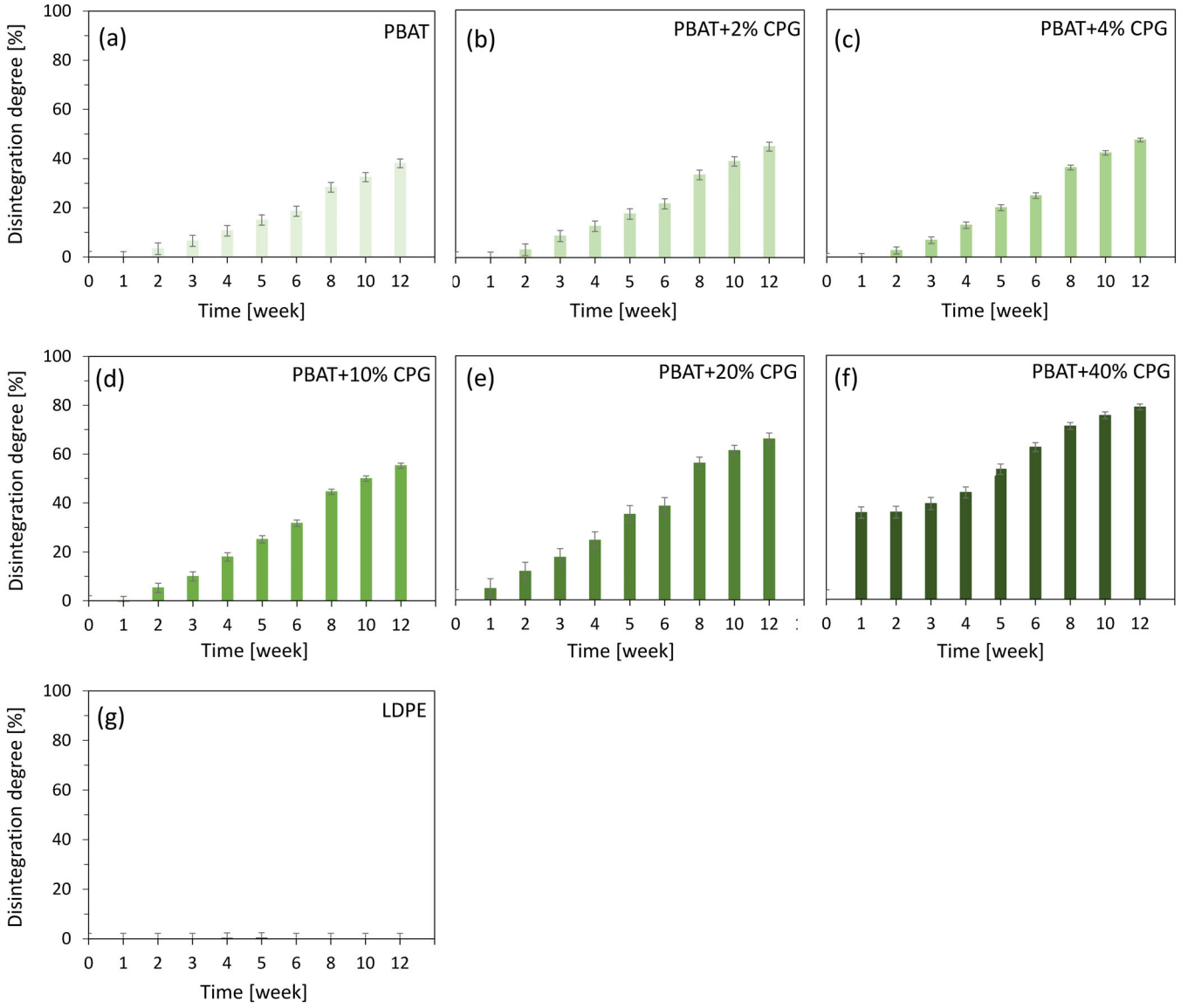

FIGURE 18 Disintegration degree for the individual tested materials as a function of time [Color figure can be viewed at wileyonlinelibrary.com]

appearance of micro cavities in the polymeric matrix, favoring the formation of attachment points by the enzymatic degradation.

In the first 2 weeks of testing, the DD variation was almost nil for about all the biocomposite materials tested. Indeed, in this initial phase the bio-oxidative degradation of the simple and immediately assimilable organic fraction can be supposed.

The PBAT+20% CPG and PBAT+40% CPG samples are the only ones to show a considerable weight reduction, most likely due to the solubilization of a part of the high phosphate glass fraction. After the first latency period, the maturation stage started and a clear increase in the DD was observed. This second phase is characterized by the biodegradation of high-molecular-weight materials and more complex molecules such as PBAT macromolecular chains and biomass present in the compost.[62]

At the end of the composting process, all bio-based composites reached a DD between 40 and 80%, with the highest DD measured for PBAT+40% CPG sample.

The DD development for the individual tested materials is made explicit in Figure 18a–g, together with the corresponding experimental errors.

As expected, LDPE was not affected by the composting conditions, showing almost complete mass conservation even after 88 days. This result supports the great difference existing between the sustainable end-of-life of the bio-based PBAT-CPG composites over a

traditional not biodegradable plastic such as LDPE, which is completely resistant to a composting process even for long periods.

At the end of test period, R value between the initial synthetic waste and the compost obtained at the end of the test was found to be greater than 50% ($R = 55 \pm 3\%$) for each reactor, thus validating the results obtained for the DD.

4 | CONCLUSION

For the first time this work proposes the preparation and characterization of biocomposite materials with a PBAT matrix reinforced with bioabsorbable CPG particles, as a valid alternative to the current materials used for agri-food packaging.

A series of composite materials was prepared by solvent casting, containing increasing CPG content from 2 up to 40 wt%.

Tensile tests revealed an effective increase in the composite stiffness compared to the pristine polymer, at the expense of yield strength, strength and elongation at break and toughness.

Experimental values of mechanical properties were validated by the Kerner's and Pukanszky's models for the estimation of the Young's modulus and of the yield and failure stresses, respectively, showing good agreement between experimental and calculated data.

IR spectra of the composites revealed no changes in the chemical structure but a decrease in the intensity of the polymer absorption peaks as the CPG concentration increased. The same behavior emerged from EDS analysis, which shows the elemental composition peaks.

From FESEM images of specimen cross-sections, it was evident that the filler particles, with an average size lower than 1 μm, are finely and homogeneously dispersed within the polymeric matrix, even at the highest concentration, without the formation of agglomerates. This confirms that the solvent casting approach is an efficient method to prepare composite materials and justifies the good correlation between the experimental data and the theoretical values of the mechanical properties, calculated through the application of theoretical models.

Furthermore, from DSC analyses, thermal properties are not significantly influenced by the addition of CPG particles as reinforcement, thus providing composites substantially the same range of applicability as the pure polymer.

Oxygen and water vapor permeability tests were carried out on films produced from each composite and on a PE film for comparison. The composites revealed a significant barrier effect against oxygen, already at the lowest concentrations of fillers, but significantly reduced against water vapor, especially when compared to the characteristic values of LDPE.

The disintegration test confirmed the high degradation difference between LDPE, a traditional thermoplastic material with no weight loss during the composting process, and the PBAT-CPG bio-composites, whose DD increased with the CPG microparticle content, up to a maximum of 80% at the end of the thermophilic incubation period. Moreover, the DD value and the resulting fragmentation rate can be modulated by varying the material composition.

According to the obtained results, CPG-filled PBAT-based composites can represent a valid biodegradable substitute for traditional thermoplastic polymeric materials, such as PE. Thanks to the similarity of PBAT performances with PE, the rigid CPG reinforcement of PBAT allows to modify and tailor the mechanical and functional properties of the material in order to expand its field of application especially in the agri-food packaging sector.

ACKNOWLEDGMENT

Open Access Funding provided by Universita degli Studi di Parma within the CRUI-CARE Agreement.

AUTHOR CONTRIBUTIONS

Corrado Sciancalepore: Conceptualization (lead); methodology (lead); writing – original draft (lead). **Elena Togliatti:** Formal analysis (lead); investigation (lead). **Alberto Giubilini:** Investigation (supporting). **Diego Pugliese:** Investigation (supporting). **Fabrizio Moroni:** Investigation (supporting). **Massimo Messori:** Resources (lead). **Daniel Milanese:** Supervision (lead); writing – review and editing (lead).

DATA AVAILABILITY STATEMENT

Research data are not shared.

ORCID

Corrado Sciancalepore https://orcid.org/0000-0002-8182-6618

REFERENCES

[1] L. Piergiovanni, S. Limbo, in *Food Packag. Mater. Tecnol. e Qual. Degli Aliment.*, Springer, Milano **2010**, p. 1. https://doi.org/10.1007/978-88-470-1457-2_1

[2] *PlasticEurope-Association of Plastics Manufactures, Plastics – The Facts 2020*, PlasticEurope, Belgium **2020**, p. 1 https://www.plasticseurope.org/en/resources/publications/4312-plastics-facts-2020

[3] D. Briassoulis, A. Giannoulis, *Polym. Test.* **2018**, *69*, 39.

[4] A. R. V. Ferreira, V. D. Alves, I. M. Coelhoso, *Membranes* **2016**, *6*, 22.

[5] D. He, Y. Luo, S. Lu, M. Liu, Y. Song, L. Lei, *TrAC - Trends Anal. Chem.* **2018**, *109*, 163.

[6] S. Spierling, E. Knüpffer, H. Behnsen, M. Mudersbach, H. Krieg, S. Springer, S. Albrecht, C. Herrmann, H. -J. Endres, *J. Cleaner Prod.* **2018**, *185*, 476.

[7] M. M. Reddy, S. Vivekanandhan, M. Misra, S. K. Bhatia, A. K. Mohanty, *Prog. Polym. Sci.* **2013**, *38*, 1653.

[8] F. V. Ferreira, L. S. Cividanes, R. F. Gouveia, L. M. F. Lona, *Polym. Eng. Sci.* **2019**, *59*, E7.

[9] E. Skoog, J. H. Shin, V. Saez-Jimenez, V. Mapelli, L. Olsson, *Biotechnol. Adv.* **2018**, *36*, 2248.

[10] R. G. C. Silva, T. F. Ferreira, É. R. Borges, *J. Chem. Technol. Biotechnol.* **2020**, *95*, 3057.

[11] M. Volanti, D. Cespi, F. Passarini, E. Neri, F. Cavani, P. Mizsey, D. Fozer, *Green Chem.* **2019**, *21*, 885.

[12] M. T. Zumstein, A. Schintlmeister, T. F. Nelson, R. Baumgartner, D. Woebken, M. Wagner, H. -P. E. Kohler, K. McNeill, M. Sander, *Sci. Adv.* **2018**, *4*, eaas9024.

[13] J. Jian, Z. Xiangbin, H. Xianbo, *Adv. Ind. Eng. Polym. Res.* **2020**, *3*, 19.

[14] J. Lunt, *Polym. Degrad. Stab.* **1998**, *59*, 145.

[15] K. O. Siegenthaler, A. Künkel, G. Skupin, M. Yamamoto, *Adv. Polym. Sci.* **2011**, *245*, 91.

[16] V. Nagarajan, M. Misra, A. K. Mohanty, *Ind. Crops Prod.* **2013**, *42*, 461.

[17] K. Oksman, Y. Aitomäki, A. P. Mathew, G. Siqueira, Q. Zhou, S. Butylina, S. Tanpichai, X. Zhou, S. Hooshmand, *Compos. Part A Appl. Sci. Manuf.* **2016**, *83*, 2.

[18] T. Burford, W. Rieg, S. Madbouly, *Phys. Sci. Rev.* **2021**. https://doi.org/10.1515/psr-2020-0078

[19] L. Botta, V. Titone, M. C. Mistretta, F. P. La Mantia, A. Modica, M. Bruno, F. Sottile, F. Lopresti, *Polymers* **2021**, *13*, 2643. https://doi.org/10.3390/polym13162643

[20] M. Mariano, C. Chirat, N. El Kissi, A. Dufresne, *J. Polym. Sci. Part B Polym. Phys.* **2016**, *54*, 2284.

[21] M. Mohammadi, M.-C. Heuzey, P. J. Carreau, A. Taguet, *Nanomaterials* **2021**, *11*, 857. https://doi.org/10.3390/nano11040857

[22] B. Dos Santos Rosa, C. Merlini, S. Livi, G. M. De Oliveira Barra, *Mater. Res.* **2019**, *22*, e20180541. https://doi.org/10.1590/1980-5373-MR-2018-0541

[23] K. Fukushima, A. Rasyida, M.-C. Yang, *Appl. Clay Sci.* **2013**, *80–81*, 291.

[24] B. Aaliya, K. V. Sunooj, M. Lackner, *Int. J. Biobased Plast.* **2021**, *3*, 40.

[25] I. F. Pinheiro, A. R. Morales, L. H. Mei, *Cellulose* **2014**, *21*, 4381.

[26] V. C. Beber, S. de Barros, M. D. Banea, M. Brede, L. H. de Carvalho, R. Hoffmann, A. R. M. Costa, E. B. Bezerra, I. D. S. Silva, K. Haag, K. Koschek, R. M. R. Wellen, *Materials* **2018**, *11*, 820. https://doi.org/10.3390/ma11050820

[27] H. Moustafa, C. Guizani, A. Dufresne, *J. Appl. Polym. Sci.* **2017**, *134*, 44498.

[28] C. Mayer-Laigle, L. Foulon, C. Denoual, M. Pernes, E. Rondet, A. Magueresse, C. Barron, A. Habrant, A. Bourmaud, G. Païs, *Ind. Crops Prod.* **2021**, *167*, 113482. https://doi.org/10.1016/j.indcrop.2021.113482

[29] C. Pavon, M. Aldas, H. de la Rosa-Ramírez, J. López-Martínez, M. P. Arrieta, *Polymers* **2020**, *12*, 2891.

[30] R. Venkatesan, N. Rajeswari, *Silicon* **2019**, *11*, 2233.

[31] R. Venkatesan, N. Rajeswari, *Polym. Bull.* **2019**, *76*, 4785.

[32] R. Venkatesan, N. Rajeswari, *Polym. Adv. Technol.* **2017**, *28*, 20.

[33] X. Wang, L. Cui, S. Fan, X. Li, Y. Liu, *Polymers* **2021**, *13*, 507.

[34] V. M. Sglavo, D. Pugliese, F. Sartori, N. G. Boetti, E. Ceci-Ginistrelli, G. Franco, D. Milanese, *J. Alloys Compd.* **2019**, *778*, 410.

[35] E. Ceci-Ginistrelli, D. Pugliese, N. G. Boetti, G. Novajra, A. Ambrosone, J. Lousteau, C. Vitale-Brovarone, S. Abrate, D. Milanese, *Opt. Mater. Express* **2016**, *6*, 2040. https://doi.org/10.1364/ome.6.002040

[36] J. C. Knowles, *J. Mater. Chem.* **2003**, *13*, 2395.

[37] F. Ruggero, R. Gori, C. Lubello, *Waste Manage. Res.* **2019**, *37*, 959.

[38] J. Ahrens, B. Geveci, C. Law, *The Visualization Handbook*, Elsevier, Amsterdam, Netherlands **2005**, Ch. 36, p. 717. https://doi.org/10.1016/B978-012387582-2/50038-1

[39] T. B. Lewis, L. E. Nielsen, *J. Appl. Polym. Sci.* **1970**, *14*, 1449.

[40] L. Százdi, B. Pukánszky, G. J. Vancso, B. Pukánszky, *Polymer* **2006**, *47*, 4638.

[41] J. Móczó, B. Pukánszky, *J. Ind. Eng. Chem.* **2008**, *14*, 535.

[42] R. F. Landel, L. E. Nielsen, *Mechanical Properties of Polymers and Composites*, 2nd ed., Taylor & Francis, New York **1993**. https://books.google.it/books?id=Q-d50ibrGiUC

[43] A. Lazzeri, V. T. Phuong, *Compos. Sci. Technol.* **2014**, *93*, 106.

[44] G. Faludi, G. Dora, K. Renner, J. Móczó, B. Pukánszky, *Carbohydr. Polym.* **2013**, *92*, 1767.

[45] B. Pukánszky, *Composites* **1990**, *21*, 255.

[46] A. Giubilini, C. Sciancalepore, M. Messori, F. Bondioli, *J. Appl. Polym. Sci.* **2020**, *137*, 48953.

[47] A. Giubilini, C. Sciancalepore, M. Messori, F. Bondioli, *J. Mater. Cycles Waste Manag.* **2021**, *23*, 402.

[48] R. Taurino, C. Sciancalepore, L. Collini, M. Bondi, F. Bondioli, *Compos. Part B: Eng.* **2018**, *149*, 240.

[49] A. Galeski, *Prog. Polym. Sci.* **2003**, *28*, 1643.

[50] K. Renner, C. Kenyó, J. Móczó, B. Pukánszky, *Compos. Part A Appl. Sci. Manuf.* **2010**, *41*, 1653.

[51] S. N. Maiti, K. K. Sharma, *J. Mater. Sci.* **1992**, *27*, 4605.

[52] S. Paszkiewicz, A. Szymczyk, D. Pawlikowska, I. Irska, I. Taraghi, R. Pilawka, J. Gu, X. Li, Y. Tu, E. Piesowicz, *RSC Adv.* **2017**, *7*, 41745.

[53] L. Baia, D. Muresan, M. Baia, J. Popp, S. Simon, *Vib. Spectrosc.* **2007**, *43*, 313.

[54] S. Beigoli, A. Hekmat, F. Farzanegan, M. Darroudi, *J. Sol-Gel Sci. Technol.* **2021**, *98*, 508.

[55] C. Yan, Y. Zhang, Y. Hu, Y. Ozaki, D. Shen, Z. Gan, S. Yan, I. Takahashi, *J. Phys. Chem. B* **2008**, *112*, 3311.

[56] Y. Cai, J. Lv, J. Feng, *J. Polym. Environ.* **2013**, *21*, 108.

[57] G. Socrates, *Infrared Characteristic Group Frequencies: Tables and Charts*, John Wiley & Sons, Hoboken, NJ **1994**.

[58] L. Lai, S. Wang, J. Li, P. Liu, L. Wu, H. Wu, J. Xu, S. J. Severtson, W. -J. Wang, *Carbohydr. Polym.* **2020**, *247*, 116687. https://doi.org/10.1016/j.carbpol.2020.116687

[59] Z. C. Lule, E. Wondu Shiferaw, J. Kim, *Polymers* **2020**, *12*, 418. https://doi.org/10.3390/polym12020418

[60] L. W. McKeen, *Polyolefins, Polyvinyls, and Acrylics*, Elsevier, New York **2012**. doi:https://doi.org/10.1016/b978-1-4377-3469-0.10009-8.

[61] L.-F. Wang, J.-W. Rhim, S.-I. Hong, *LWT - Food Sci. Technol.* **2016**, *68*, 454.
[62] A. Giubilini, G. Siqueira, F. J. Clemens, C. Sciancalepore, M. Messori, G. Nyström, F. Bondioli, *ACS Sustain Chem. Eng.* **2020**, *8*, 10292.
[63] R. Herrera, L. Franco, A. Rodríguez-Galán, J. Puiggalí, *J. Polym. Sci. Part A Polym. Chem.* **2002**, *40*, 4141.

How to cite this article: C. Sciancalepore, E. Togliatti, A. Giubilini, D. Pugliese, F. Moroni, M. Messori, D. Milanese, *J. Appl. Polym. Sci.* **2022**, e52370. https://doi.org/10.1002/app.52370